Model bridging chimera state and explosive synchronization

Xiyun Zhang,[1] Hongjie Bi,[1] Shuguang Guan,[1] Jinming Liu,[2] and Zonghua Liu[1,2,*]
[1]*Department of Physics, East China Normal University, Shanghai 200062, China*
[2]*State Key Laboratory of Precision Spectroscopy, East China Normal University, Shanghai 200062, China*
(Received 24 January 2016; revised manuscript received 10 June 2016; published 5 July 2016)

Global synchronization and partial synchronization are the two distinctive forms of synchronization in coupled oscillators and have been well studied in recent decades. Recent attention on synchronization is focused on the chimera state (CS) and explosive synchronization (ES), but little attention has been paid to their relationship. Here we study this topic by presenting a model to bridge these two phenomena, which consists of two groups of coupled oscillators, and its coupling strength is adaptively controlled by a local order parameter. We find that this model displays either CS or ES in two limits. In between the two limits, this model exhibits both CS and ES, where CS can be observed for a fixed coupling strength and ES appears when the coupling is increased adiabatically. Moreover, we show both theoretically and numerically that there are a variety of CS basin patterns for the case of identical oscillators, depending on the distributions of both the initial order parameters and the initial average phases. This model suggests a way to easily observe CS, in contrast to other models having some (weak or strong) dependence on initial conditions.

DOI: 10.1103/PhysRevE.94.012204

I. INTRODUCTION

Synchronization in coupled oscillators has been well studied in recent decades and is now focused on the influence of network structures [1–3]. In this field, two hot topics are the chimera state (CS) and explosive synchronization (ES). CS was first found by Kuramoto and Battogtokh [4]. Following its discovery, CS has attracted a lot of attention in the past decade [5–17]. Generally speaking, CS is the coexistence of coherent and incoherent behaviors in coupled identical oscillators. Because of different initial conditions, the nonlocally coupled oscillators naturally evolve into distinct coherent and incoherent groups. This counterintuitive coexistence of coherent and incoherent oscillations in populations of identical oscillators, each with an equivalent coupling structure, can be considered a symmetry break on the collective behavior by nonsymmetric initial conditions. This phenomenon reminded people of the two-headed monster in Greek mythology and thus was named the *chimera state* by Abrams and Strogatz [18]. The study of CS was originally motivated by the phenomenon of unihemispheric sleep of many creatures in the real world [19–23], which was first found in dolphins and was then revealed in birds, some aquatic mammals, and reptiles. So far, CS has been confirmed in many experiments [24–30]. For example, Tinsley *et al.* reported on experimental studies of CS in populations of coupled chemical oscillators [24]. Hagerstrom *et al.* showed experimental observation of CS in coupled-map lattices [25]. Viktorov *et al.* demonstrated the coexistence of coherent and incoherent modes in the optical comb generated by a passively mode-locked quantum dot laser [26]. Wickramasinghe and Kiss presented an experiment of CS in a network of electrochemical reactions [27]. Martens *et al.* devised a simple experiment with mechanical oscillators to show CS [28]. And Schoenleber *et al.* reported the CS in the oxide layer during the oscillatory photoelectrodissolution of n-type doped silicon electrodes under limited illumination [30].

ES represents the first-order synchronization transition in networked oscillators. When we increase the coupling strength adiabatically, the system stays unsynchronized until a critical forward coupling strength λ_{cF} where the system suddenly becomes synchronized. That is, its order parameter R has a jump at λ_{cF}. However, when we decrease the coupling strength adiabatically from a synchronized state, the system does not go back by the same route as the forward process but jumps at a different critical backward coupling strength λ_{cB}. As $\lambda_{cF} > \lambda_{cB}$, the forward and backward routes of R form a hysteresis loop. This first-order transition was, in fact, found before the concept of complex networks [31–33] and became a hot topic only when it was rediscovered from the positive correlation between the natural frequency of a networked oscillator and its degree by Gómez-Gardeñes *et al.* and named *explosive synchronization* [34]. Before the work in [34], synchronization on complex networks was generally analyzed using the approach of the master stability function [35], which always predicts a second-order phase transition. However, [34] showed that it is also possible for the synchronization on complex networks to be the first order, thus focusing great attention on ES [36–48]. It was revealed that in addition to the way in [34], ES can also be observed in many other ways, provided that the growth of synchronized clusters is suppressed [43].

Currently, CS and ES are separately studied as two distinctive topics. In general, we do not have CS in the systems of ES and vice versa. Thus, it is interesting to ask whether it is possible to observe both of them in a single system. To figure out the answer, here we study this topic by presenting a model to bridge these two phenomena. The model consists of two groups of coupled nonidentical oscillators with a natural frequency distribution. Specifically, its coupling strength is adaptively controlled by a parameter β. This model goes back to the standard CS model [21] when all the natural frequencies are the same and $\beta = 0$ and returns to the adaptive model of ES [48] when there is only one group of oscillators and $\beta = 1$. Very interesting, we find that this model displays both CS and ES, where CS can be observed for a fixed coupling strength and

*zhliu@phy.ecnu.edu.cn

ES appears when the coupling is increased adiabatically. Thus, this model sets up a bridge between CS and ES. Moreover, we focus on the case of identical oscillators and show both theoretically and numerically that there are a variety of CS basin patterns, depending on the distributions of both the initial order parameters and the initial average phases. That is, this model shows a way to easily observe CS, in contrast to the sensitive dependence on initial conditions in many previous models [49,50].

This paper is organized as follows. In Sec. II, we introduce the model and study its collective behaviors. In Sec. III, we pay attention to the case of identical oscillators and study it using the dimensional reduction analysis. In Sec. IV, we show the corresponding numerical simulations and their stability analysis. Finally, in Sec. V, we give conclusions and a discussion.

II. MODEL DESCRIPTION

We consider a model of two groups of coupled oscillators, defined as

$$\dot{\theta}_{i,j} = \omega_{i,j} + \frac{R_j^\beta \lambda}{N}\sum_{k=1}^{N}\sin(\theta_{k,j} - \theta_{i,j} + \alpha) + \frac{R_j^\beta \lambda'}{N}\sum_{k=1}^{N}\sin(\theta_{k,j'} - \theta_{i,j} + \alpha), \quad (1)$$

where the index $j = 1,2$ represents the two groups and $i = 1,\ldots,N$ represents the N oscillators in each group. $\omega_{i,j}$ is the natural frequency satisfying a uniform distribution in $(-\delta,\delta)$. The oscillators are globally coupled with coupling strength λ inside each group and coupling strength λ' between the two groups. j' represents the other group, defined as $j' = 2$ when $j = 1$ and $j' = 1$ when $j = 2$. α is a phase lag parameter and is set as $\alpha = \frac{\pi}{2} - 0.1$, which was chosen by many CS papers [21–23]. The coupling is attractive when $\alpha < \pi/2$ and repulsive when $\alpha > \pi/2$. β is a parameter located in $[0,1]$.

R_1 and R_2 in Eq. (1) are the order parameters of groups 1 and 2, respectively, which are defined as

$$R_1 e^{i\Psi_1} = \frac{1}{N}\sum_{k=1}^{N} e^{i\theta_{k,1}}, \quad R_2 e^{i\Psi_2} = \frac{1}{N}\sum_{k=1}^{N} e^{i\theta_{k,2}}. \quad (2)$$

In the framework of Eq. (1), the population is put into two groups, and the coupling strengths $R_j^\beta\lambda$ and $R_j^\beta\lambda'$ are closely correlated to the local coherence when β is not zero. The model (1) will return to the case of one population in Ref. [48] when $\lambda' = 0$ and $\beta = 1$. To show the influence of β, Fig. 1 shows the synchronization transition of model (1) for different β, with $\lambda' = 0$. It is easy to see that R has a continuous transition for $\beta = 0$, a discontinuous transition for $\beta = 1$, and a transition gradually changing from continuous to discontinuous when β increases, indicating a transition from traditional synchronization to explosive synchronization. When β is in the range of the hysteresis loop, there is bistability where the final state of system depends sensitively on the initial conditions.

The model (1) is more sensitive to the local coherence if there are two or more groups in the system. Once the initial conditions are asymmetric, the two groups may easily go to different final states, i.e., one group with high coherence and another group with low coherence.

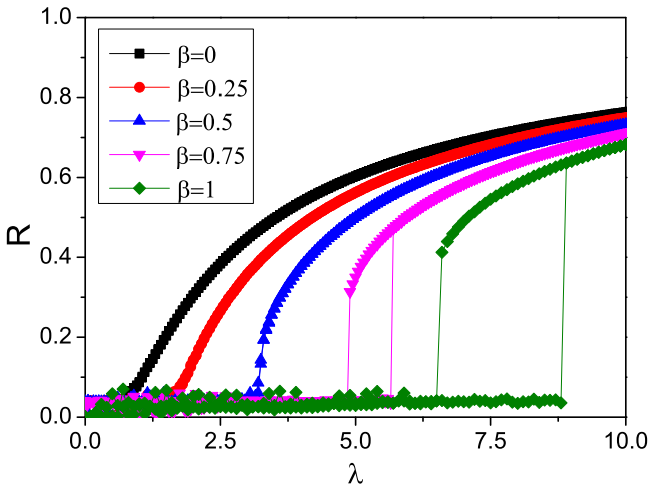

FIG. 1. Synchronization transition of model (1) with only one population, i.e., $\lambda' = 0$. The parameters are $\delta = 1.0$ and $\alpha = \frac{\pi}{2} - 0.1$

Equation (1) has two limiting behaviors. The first one is the limiting behavior of $\lambda' = 0$ and $\beta = 1$, which goes back to the adaptive model of ES in Ref. [48]. In this situation, ES can be observed if we increase (decrease) the coupling adiabatically in the forward (backward) continuation diagram. Figure 2(a) shows the dependence of R_1 on λ for $\delta = 1.0$. It is easy to see that there is a hysteresis loop, indicating the existence of ES. The inset of Fig. 2(a) shows the evolution of two different initial conditions for $\lambda = 8.5$. We see that one gradually approaches a higher value ($R_1 \approx 0.58$) and the other

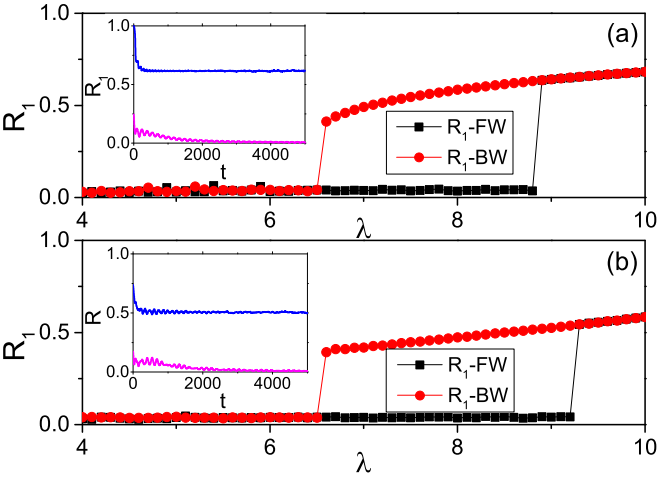

FIG. 2. (a) Case of $\lambda' = 0$ with $\delta = 1.0, \alpha = \frac{\pi}{2} - 0.1$, and $\beta = 1$. The squares and circles represent R_1 for the forward and backward continuation diagrams, respectively. The inset shows the evolution of two different initial conditions for $\lambda = 8.5$. (b) Case of $\lambda' = 2$ with $\delta = 1.0, \alpha = \frac{\pi}{2} - 0.1$, and $\beta = 1$. The squares and circles represent R_1 for the forward and backward continuation diagrams (R_2 has the same loop but is not shown here), respectively. The two curves in the inset show the evolution of typical R_1 and R_2 in the two groups, respectively, with $\lambda = 8.5$.

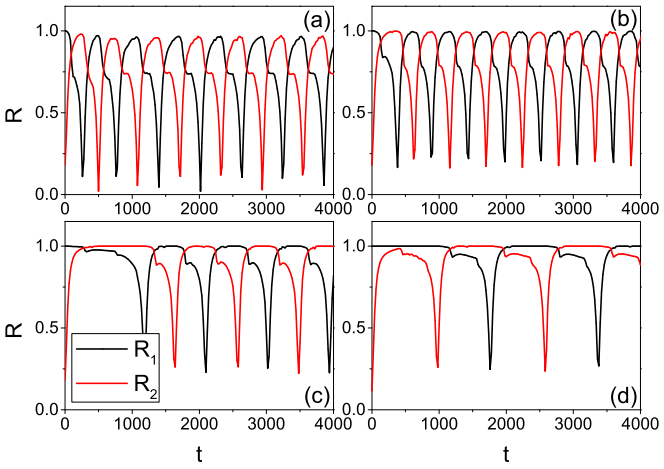

FIG. 3. The chimera-like behaviors in Eq. (1) for $\beta = 0, \lambda = 8.0$, and $\lambda' = 3.0$, where the black and red lines represent R_1 and R_2, respectively, and (a)–(d) represent the cases of $\delta = 1.0, 0.5, 0.2$, and 0.15, respectively.

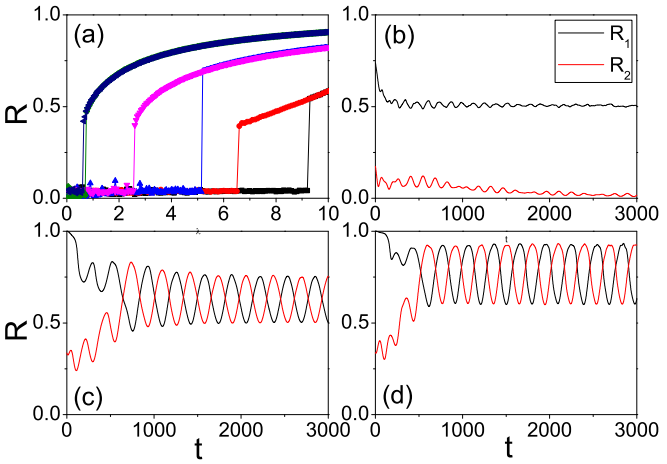

FIG. 4. Coexistence of ES and CS in the model of Eq. (1) for $\alpha = \frac{\pi}{2} - 0.1, \beta = 1$, and $\lambda' = 2$. (a) R_1 versus λ, where the black and red lines represent R_1 of the forward and backward continuation diagrams for $\delta = 1$, respectively; the blue and pink lines represent the case of $\delta = 0.7$, and the dark green and dark blue lines represent the case of $\delta = 0.4$. (b)–(d) Evolutions of R_1 and R_2 on time t for $\lambda = 8.0$ and $\delta = 1, 0.7$, and 0.4, respectively.

goes to zero, confirming the sensitivity to initial conditions in the bistable region. We have the same results for R_2 of another group (it is not shown in Fig. 2), as the system exhibits the symmetry $1 \leftrightarrow 2$.

The second one is the limiting behavior of identical $\omega_{i,j}$ ($\delta = 0$) in Eq. (1) for all the oscillators and $\beta = 0$, which returns to the typical model of CS in Ref. [21]. In this case, our numerical simulations confirm that one group is synchronized with $R_1 = 1$, while the other is unsynchronized with $R_2 < 1$. Furthermore, we were surprised to find that there is still a chimera-like behavior when we keep $\beta = 0$ but let $\omega_{i,j}$ satisfy the uniform distribution in $(-\delta, \delta)$. Figures 3(a)–3(d) show the results for $\delta = 1.0, 0.5, 0.2$, and 0.15, respectively. We see that the oscillation periods of R_1 and R_2 increase with the decrease of δ until $\delta = 0.15$. After that, the oscillation behaviors of R_1 and R_2 will disappear and are replaced by one group being synchronized and the other being unsynchronized, i.e., the chimera state.

We now go back to the current model of Eq. (1) with $\beta = 1$. We find that it can also show the hysteresis loop. Figure 2(b) shows the results of R_1 for $\lambda' = 2$. Comparing Fig. 2(b) with Fig. 2(a), we see that their forward jumping positions are slightly different, i.e., $\lambda_{cF} < 9.0$ in Fig. 2(a), while $\lambda_{cF} > 9.0$ in Fig. 2(b). We have observed the same results for R_2 (not shown here), as the symmetry $1 \leftrightarrow 2$ in the two groups of the system. The inset of Fig. 2(b) shows the evolution of two typical initial conditions from the two groups for $\lambda = 8.5$. We see that one (R_1) goes to a higher value ($R_1 \approx 0.58$) and the other (R_2) goes to zero, indicating a chimera-like behavior. Therefore, we have observed both ES and CS in the model of Eq. (1) when the parameters are taken in the range of the hysteresis loop.

Then, we change the range of frequency distribution δ. We find that the hysteresis loop depends on the parameter δ and can be observed only when $\delta > 0.31$. With the decrease of δ, the size of the loop decreases until zero at about $\delta = 0.31$, and the transition points of R_1 or R_2 also approach zero. Figure 4(a) shows the results for $\lambda' = 2$, where the squares and circles represent R_1 of the forward and backward continuation diagrams for $\delta = 1$, respectively; the upward triangles and downward triangles represent the case of $\delta = 0.7$, and the diamonds and leftward triangles represent the case of $\delta = 0.4$. To check the coexistence of CS, we study the evolution of R_1 and R_2 for two different initial conditions. Figures 4(b)–4(d) show the results for $\lambda = 8.0$ and $\delta = 1, 0.7$, and 0.4, respectively. We see that Fig. 4(b) is a chimera-like state, while Figs. 4(c) and 4(d) are breather-like states. In sum, the range of frequency distribution δ takes a key role for the coexistence of ES and CS.

III. DIMENSIONAL REDUCTION ANALYSIS

In the following, we study CS in model (1) with $\beta = 1$. In order to satisfy the definition of CS, we change to identical oscillators ($\delta = 0$). To make a theoretical analysis of Eq. (1), it is better to reduce its dimension. Fortunately, such an approach of dimensional reduction was proposed by Watanabe and Strogatz [51] and then generalized by Pikovsky and Rosenblum [22]. Here we adopted it to analyze the model (1). In a mean-field framework, the coupling terms in Eq. (1) can be rewritten as $R_a^2 \lambda \sin(\Psi_a - \theta_j^a + \alpha) + R_a R_{a'} \lambda' \sin(\Psi_{a'} - \theta_j^a + \alpha)$. Thus, Eq. (1) can be rewritten as

$$\begin{aligned} \dot{\theta}_j^a &= \mathrm{Im}(Z_a e^{-i\theta_j^a}), \\ Z_a &= R_a^2 \lambda e^{-i(\Psi_a + \alpha)} + R_a R_{a'} \lambda' e^{-i(\Psi_{a'} + \alpha)}, \end{aligned} \tag{3}$$

where Z is the mean field coupling for oscillator j and a and a' are the indices of the two populations, respectively. The average frequency $\langle \omega \rangle$ has been ignored as it is zero for a symmetric distribution. By introducing the variables $\rho_a(t)$, $\Theta_a(t)$, and $\Phi_a(t)$ and constants ψ_j^a via the transformation

$$\tan\left[\frac{\theta_j^a - \Phi_a}{2}\right] = \frac{1 - \rho_a}{1 + \rho_a} \tan\left[\frac{\psi_j^a - \Theta_a}{2}\right], \tag{4}$$

we get the Watanabe-Strogatz equations of the Eq. (1) [22,51],

$$\dot{\rho}_a = \frac{1-\rho_a^2}{2}\mathrm{Re}(Z_a e^{-i\Phi_a}),$$
$$\dot{\Theta}_a = \frac{1-\rho_a^2}{2\rho_a}\mathrm{Im}(Z_a e^{-i\Phi_a}),$$
$$\dot{\Phi}_a = \frac{1+\rho_a^2}{2\rho_a}\mathrm{Im}(Z_a e^{-i\Phi_a}). \quad (5)$$

Generally, the parameter ρ characterizes the degree of synchronization: $\rho = 0$ if the oscillators are incoherent, and $\rho = 1$ if the oscillators are completely synchronized. ρ_a is roughly proportional to the order parameter R_a. The phase variable Θ describes the shift of individual oscillators with the mean phase, and Φ describes the average of the phases. It is convenient to introduce new variables $\xi_a = \Phi_a - \Theta_a$ and $z_a = \rho_a e^{i\Phi_a}$; then Eq. (5) can be rewritten as

$$\dot{z}_a = \frac{1}{2}Z_a - \frac{z_a^2}{2}Z_a^*, \quad (6)$$
$$\dot{\xi}_a = \mathrm{Im}(z_a^* Z_a). \quad (7)$$

If the constants ψ_j^a are uniformly distributed, Eqs. (6) and (7) will decouple. Equation (6) describes the low-dimensional behavior of Eq. (1). In the thermodynamic limit, we have $\rho_a = R_a$, and thus, from Eq. (6) we obtain

$$\dot{R}_a = \tfrac{1}{2}R_a\left(1-R_a^2\right)[\lambda R_a\cos\alpha + \lambda' R_{a'}\cos(\Phi_{a'} - \Phi_a + \alpha)],$$
$$\dot{\Phi}_a = \tfrac{1}{2}\left(1+R_a^2\right)[\lambda R_a\sin\alpha + \lambda' R_{a'}\sin(\Phi_{a'} - \Phi_a + \alpha)]. \quad (8)$$

Equation (8) describes the theoretical prediction of the collective behaviors of Eq. (1). However, it is not easy to get the precise solution of Eq. (8). Hence, we calculate Eq. (1) numerically. In this way, the initial order parameters $R_1(0)$ and $R_2(0)$ and the initial phases $\Phi_1(0)$ and $\Phi_2(0)$ will be the key factors influencing the final states R_1 and R_2.

IV. RESULTS AND ANALYSIS

In numerical simulations, we take the system size as $2N = 100$, i.e., $N = 50$ for each group. For the convenience of making a comparison with the above theoretical predictions, we let all the natural frequencies $\omega_{i,j}$ in Eq. (1) be zero. The initial phases are drawn from the circular Cauchy distribution [52]

$$g(\theta(0)) = \frac{1-|\gamma|^2}{2\pi|e^{i\theta}-\gamma|^2}, \quad (9)$$

which can be easily generated from a Lorentzian distribution $g(x) = \frac{1}{\pi}[\frac{\eta}{(x-x_0)^2+\eta^2}]$, with η being the half width at half maximum and x_0 being the center frequency. Making a transformation $X = \frac{x+i}{x-i}$, we can get a new complex variable X, which is distributed on a unit circular in the complex plane. The phases of X are distributed as the circular Cauchy distribution. By changing x_0 and η, we can easily change the average and deviation of the circular Cauchy distribution and thus change the initial order parameter of the oscillators. In this way, we have observed a variety of CS patterns in the two groups. Figures 5(a) and 5(b) show two typical CS patterns after the transient process, where Fig. 5(a) denotes the case of coupling strength $\lambda = \lambda' = 1$ and the initial order parameter $R_1(0) = 0.275$ and $R_2(0) = 0.569$ and Fig. 5(b) denotes the case of coupling strength $\lambda = 1.5$ and $\lambda' = 1$ and the initial order parameters $R_1(0) = 0.1$ and $R_2(0) = 0.569$. We see that in each case, one group is synchronized with $R_2 = 1$, and the other has a different $R_1 < 1$, implying a breathing CS. In contrast, we numerically calculate the theoretical equation (8) and show the results in Figs. 5(c) and 5(d), where the difference between the initial phases of the two groups is taken as $\Delta\Phi = \Phi_2(0) - \Phi_1(0) = 2\pi/3$. In fact, Figs. 5(c) and 5(d) can be considered the corresponding theoretical results of Figs. 5(a) and 5(b). Comparing Fig. 5(a) with Fig. 5(c) and Fig. 5(b) with Fig. 5(d), we see that the theoretical results are qualitatively consistent with the numerical simulations.

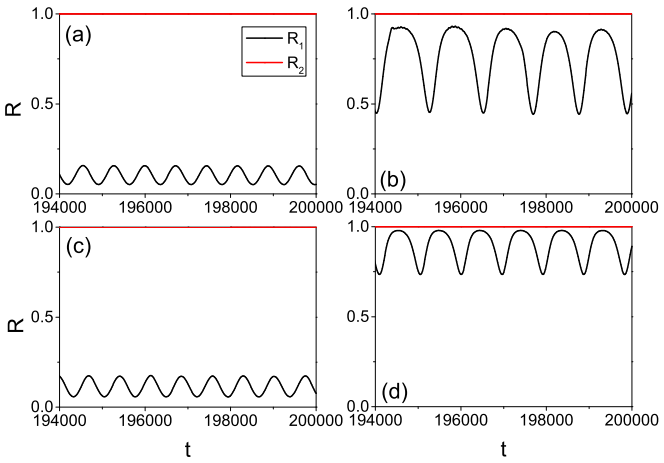

FIG. 5. Comparison between numerical simulations and theoretical results, where (a) and (b) represent the numerical simulations from Eq. (1) with $\omega_{i,j} = 0$ and (c) and (d) represent the corresponding theoretical results from Eq. (8). (a) and (c) The coupling strength is $\lambda = \lambda' = 1$, and the initial order parameters are taken as $R_1(0) = 0.275$ and $R_2(0) = 0.569$. The difference between the initial average phase is $\Delta\Phi = \Phi_2(0) - \Phi_1(0) = 2\pi/3$. (b) and (d) The coupling strengths are $\lambda = 1.5$ and $\lambda' = 1$, and the initial order parameters are taken as $R_1(0) = 0.1$ and $R_2(0) = 0.569$. The difference between the initial average phases is also taken as $\Delta\Phi = \Phi_2(0) - \Phi_1(0) = 2\pi/3$.

To show the dependence of CS on the initial conditions in detail, we first fix the initial average phases as $\Delta\Phi = \Phi_2(0) - \Phi_1(0) = 2\pi/3$ and let the initial order parameters $R_1(0)$ and $R_2(0)$ gradually increase from 0 to 1 by changing x_0 and η. Figures 6(a) and 6(b) show how the stabilized R_1 and R_2 depend on the initial $R_1(0)$ and $R_2(0)$. Comparing Fig. 6(a) with Fig. 6(b), we see that R_1 is low when R_2 is high and vice versa; that is, they are complementary, indicating that the whole system is always in CS. This is an interesting finding which tells us that no matter what the initial conditions are, we can always find one group that has high coherence while the other has low coherence, indicating that the basin of CS in the model of Eq. (1) is the whole initial condition space or CS is robust to initial conditions. This feature is very different from some of the previous models of CS, where CS is typically observed for carefully chosen initial conditions. We also show the corresponding theoretical results from Eq. (8) in Figs. 6(c) and 6(d). Comparing Fig. 6(a) with Fig. 6(c) and Fig. 6(b) with Fig. 6(d), we see that they are almost the same, indicating the

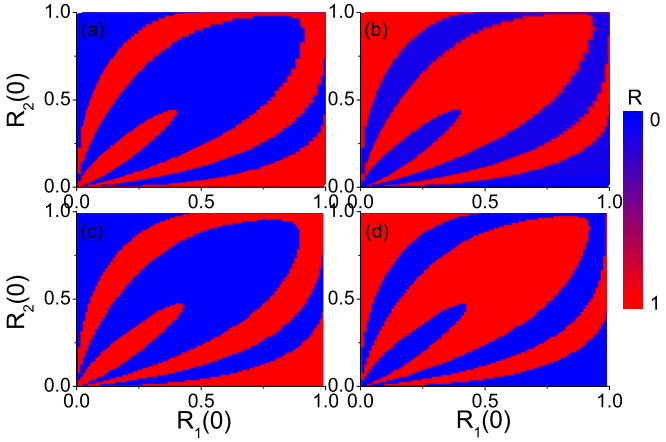

FIG. 6. Influence of the initial order parameters $R_1(0)$ and $R_2(0)$ on the stabilized R_1 and R_2 in the two groups. (a) and (b) show the results of numerical simulations for R_1 and R_2 from Eq. (1), respectively. (c) and (d) show the theoretical results from Eq. (8), corresponding to (a) and (b), respectively. The differences between the initial average phases are all $\Delta\Phi = 2\pi/3$, and the coupling strength is $\lambda = \lambda' = 1$.

consistence between the numerical simulations and theoretical results.

Then, we study the influence of the initial average phases. For this purpose, we consider a variety of differences $\Delta\Phi = \Phi_2(0) - \Phi_1(0)$. As $\Delta\Phi$ is not neglected in Eq. (8) of the dimensional reduction, the low-dimensional analysis shows the same effect as the numerical simulations by the circular Cauchy distributed initial conditions. For this reason, here we only calculate the theoretical solution of Eq. (8). We find that the stabilized CS does depend on the specific values of the initial average phases. As R_1 and R_2 are complementary, we only calculate the stabilized R_1. Figure 7 shows four typical cases, where Figs. 7(a)–7(d) represent the cases with $\Delta\Phi = \pi/3, \pi, \pi/2$ and 0, respectively. It is easy to see that the four patterns in Fig. 7 are different, indicating the diversity of the CS basin patterns for different initial conditions.

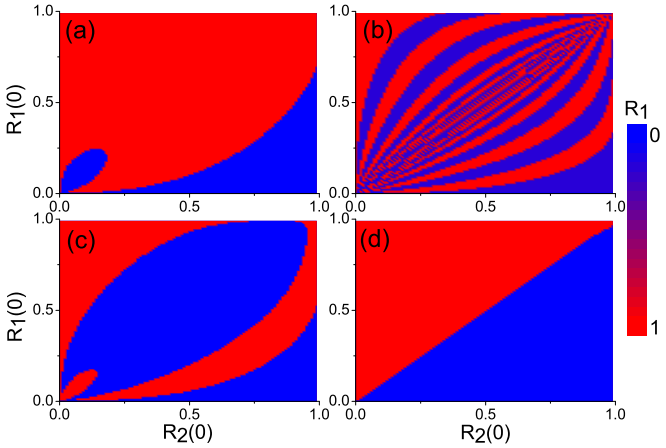

FIG. 7. Influence of different initial average phases $\Delta\Phi = \Phi_2(0) - \Phi_1(0)$ on the patterns of CS, where the parameters are the same as in Fig. 6. The results are obtained for the stationary R_1 by the theoretical analysis (8). (a) Case of $\Delta\Phi = \pi/3$. (b) Case of $\Delta\Phi = \pi$. (c) Case of $\Delta\Phi = \pi/2$. (d) Case of $\Delta\Phi = 0$.

The robustness of CS to initial conditions is very interesting. To understand it better, we follow Ref. [21] to make a further analysis of Eq. (8). First, we introduce a new parameter $A = \lambda - \lambda'$. As all the frequencies of oscillators are zero, we rescale the coupling as $1 = \lambda + \lambda'$ and thus obtain $\lambda = (1 + A)/2$ and $\lambda' = (1 - A)/2$. Therefore, $A = 0$ represents the case of $\lambda = \lambda'$, while $A = 1$ represents the case of $\lambda' = 0$, i.e., only one group of the population. Then, we introduce $\Delta\Phi = \Phi_2 - \Phi_1$. For a typical CS, one population is synchronized with $R = 1$; thus, we can set its order parameter as unity, i.e., $R_1 = 1$ and $\dot{R}_1 = 0$. In this way, Eq. (8) becomes

$$\begin{aligned}
\dot{R}_2 &= \frac{1}{2}R_2\left(1 - R_2^2\right)\left[\frac{1+A}{2}R_2\cos\alpha\right. \\
&\quad \left. + \frac{1-A}{2}\cos\left(-\Delta\Phi + \alpha\right)\right], \\
\Delta\dot{\Phi} &= \frac{1}{2}\left(1 + R_2^2\right)\left[\frac{1+A}{2}R_2\sin\alpha + \frac{1-A}{2}\sin\left(-\Delta\Phi + \alpha\right)\right] \\
&\quad - \left[\frac{1+A}{2}\sin\alpha + \frac{1-A}{2}R_2\sin\left(\Delta\Phi + \alpha\right)\right]. \qquad (10)
\end{aligned}$$

By letting $\dot{R}_2 = 0$, we can get three solutions: $R_2 = 1$, $R_2 = 0$, and $R_2 = -\frac{(1-A)\cos(\alpha-\Delta\Phi)}{(1+A)\cos\alpha}$. The first solution means a complete synchronized state, and the other two mean CS. By checking the values of R_1 and R_2 in both Figs. 6 and 7, we find that all the blue areas are in between 0.1 and 0.2, indicating that they are the third solution. Therefore, we focus only on the first two solutions, i.e., $R_2 = 1$ and $R_2 = 0$. The Jacobian matrix of Eq. (10) is

$$M = \begin{bmatrix} a & b \\ c & d \end{bmatrix}, \qquad (11)$$

with

$$\begin{aligned}
a &= \frac{1+A}{2}R_2\cos\alpha + \frac{1-A}{4}\cos\left(\alpha - \Delta\Phi\right) \\
&\quad -(1+A)R_2^3\cos\alpha - \frac{3(1-A)}{4}R_2^2\cos\left(\alpha - \Delta\Phi\right), \\
b &= \frac{1}{2}R_2\left(1 - R_2^2\right)\sin\left(\alpha - \Delta\Phi\right), \\
c &= \frac{1+A}{4}\sin\alpha + \frac{3(1+A)}{4}R_2^2\sin\alpha \\
&\quad + \frac{1-A}{2}R_2\sin\left(\alpha - \Delta\Phi\right) - \frac{1-A}{2}\sin\left(\Delta\Phi + \alpha\right), \\
d &= -\frac{1-A}{4}\left(1 + R_2^2\right)\cos\left(\alpha - \Delta\Phi\right) \\
&\quad - \frac{1-A}{2}R_2\cos\left(\Delta\Phi + \alpha\right). \qquad (12)
\end{aligned}$$

By using the linear stability analysis we find that the solution of $R_2 = 0$ is unstable, while $R_2 = 1$ is stable with the same parameters as in Figs. 6 and 7. This means that there is a probability to observe the complete synchronization in the initial condition space. With further linear stability analysis, we find that the invariant manifold with $R_1 = R_2$ found in [49] still exists. In order to check this point, we fix the average of initial order $\langle R(0)\rangle = [R_1(0) + R_2(0)]/2$ and look for the basin of the states in the plane of $\Delta R(0) = R_1(0) - R_2(0)$

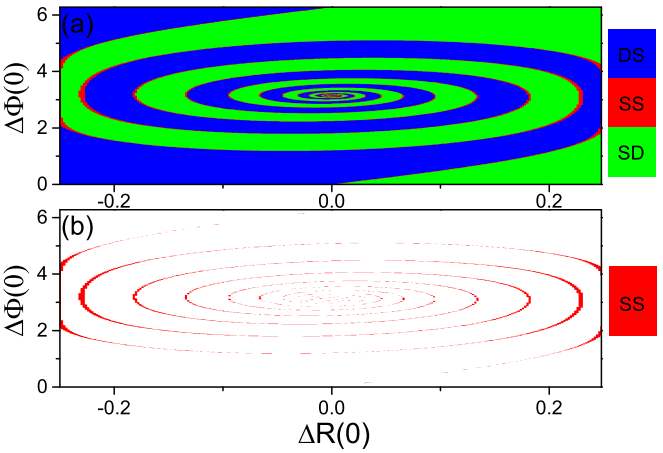

FIG. 8. Influence of the initial order parameters, $\Delta R(0)$ and $\Delta\Phi(0)$, on the stabilized R_1 and R_2 in the two groups with the same parameters as in Figs. 6 and 7, i.e., $A = 0$. The average of the initial order parameter is $\langle R(0)\rangle = [R_1(0) + R_2(0)]/2 = 0.75$. Results are obtained by solving Eq. (10). (a) shows the distribution of the stabilized state, where DS means the first group is synchronized while the second group is desynchronized, SD means the second group is synchronized while the first group is desynchronized, and SS means both groups are synchronized. (b) shows only the basin of the completely synchronized state, while the basin of CS is hidden.

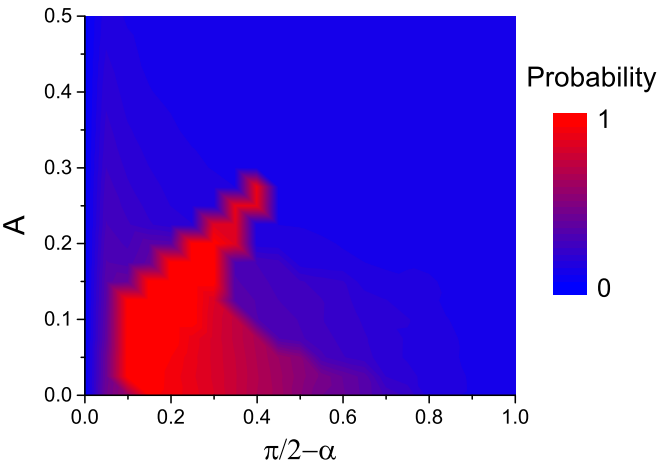

FIG. 9. Probability of CS when using different initial conditions in the case of different A and α, where the results are obtained by solving the Eq. (10).

and $\Delta\Phi(0)$, i.e., following the same steps as Ref. [49]. Figure 8(a) shows the distribution of the stabilized state for the case of $\langle R(0)\rangle = 0.75$, where DS means the first group is synchronized while the second one is desynchronized, SD means the second group is synchronized while the first one is desynchronized, and SS means both groups are synchronized. Thus, DS and SD are CS, while SS is a completely synchronized state. From this figure, we see the basin of the completely synchronized state (SS) is very narrow, and it occurs only when the system changes from the DC state to the SD state or vice versa, which is the same as in Ref. [49]. To illustrate this more clearly, Fig. 8(b) shows only the basin of the synchronized state, where the basin of CS is hidden. These basins of the completely synchronized state are too narrow and thus make the SS state hare to observe, which is the reason why we miss the completely synchronized state in Figs. 6 and 7. On the other hand, we notice that in Fig. 8, the basins of the states are spiral shaped around the point $\Delta R(0) = 0$, $\Delta\Phi(0) = \pi$, indicating the influence of the initial phases. This is very similar to the result of Ref. [49].

In order to show how the basins of CS change with the parameters, we calculate the probability of the chimera state with different initial conditions in the parameter plane of A versus $\pi/2 - \alpha$. Figure 9 shows the results. It is easy to see that the probability of CS decreases as α decreases. When A is large, the probability of CS becomes zero.

V. DISCUSSION

To connect CS and ES, Eq. (1) has three key aspects. The first one is the asymmetric couplings λ and λ'. When $\lambda > \lambda'$, the coupling in each group is greater than that between the two groups. Thus, the oscillators may be synchronized in their own groups but remain unsynchronized to those in another group. The second one is the control parameter β. It guarantees the appearance of ES. The third one is the range parameter of the natural frequencies δ. When δ is relatively large, we have both ES and CS-like behaviors. When δ is relatively small, we only have CS. In this sense, we may also consider δ to be the parameter connecting CS and ES.

One advantage of Eq. (1) is that its CS can be easily observed. The underlying mechanism may be the bistability. It is known that CS is a kind of symmetry breaking of coherence due to the symmetry breaking in the initial conditions. If a system shows CS, its oscillators should have multistability or bistability so that the sensitivity to the initial conditions can evolve into the final coexisting behaviors of coherence and incoherence in different population groups. Thus, the multistability or bistability is the necessary condition for CS. On the other hand, a characteristic feature of ES is the existence of a hysteresis loop in the order parameter. When the coupling strength is located in this hysteresis region, the system has two stable states, one with high coherence and the other with low coherence, separated by an unstable state. When the coupling is increased adiabatically in the bistable region, the feature of low (high) coherence remains and thus results in the hysteresis loop, indicating that the bistability is also the necessary condition for ES. Therefore, the bistability is the common basis of CS and ES.

Because of the correlation between the local order parameter and the coupling strength, our model is more sensitive to symmetry breaking of the initial conditions, which makes CS easier to observe. On the other hand, we find that in our model, the basin of CS can be very large, which is similar to the large basin of CS in Refs. [49,50]. The spiral-shaped basin of states is also similar to the basin structure in [49] and reminds us of the spiral wave chimeras in [9], although they are different phenomena.

In conclusion, we have presented a model to describe both CS and ES. We reveal that in two limits, the system goes to CS or ES. In between the two limits, the model can show both CS and ES at the same coupling strength. The frequency

distribution parameter δ may seriously influence the final state. When all the natural frequencies are zero, CS is robust to the initial conditions, and thus, a diversity of the CS basin patterns can be observed. These findings have been confirmed by both numerical simulations and theoretical analysis, which improves our understanding of both CS and ES, especially their connection.

ACKNOWLEDGMENTS

X.Z. thanks Prof. A. Pikvosky for many useful discussions. The authors thank the reviewers for their valuable comments. This work was partially supported by the NNSF of China under Grants No. 11135001 and No. 11375066, the 973 Program under Grant No. 2013CB834100, and the Open Fund from the SKLPS of ECNU.

[1] A. Pikvosky, M. Rosenblum, and J. Kurths, *Synchronization: A Universal Concept in Nonlinear Sciences* (Cambridge University Press, Cambridge, 2003).
[2] S. Boccaletti, V. Latora, and Y. Moreno, Phys. Rep. **424**, 175 (2006).
[3] A. Arenas, A. Diaz-Guilera, J. Kurths, Y. Moreno, and C. Zhou, Phys. Rep. **469**, 93 (2008).
[4] Y. Kuramoto and D. Battogtokh, Nonlinear Phenom. Complex Syst. **5**, 380 (2002).
[5] O. E. Omelchenko, Y. L. Maistrenko, and P. A. Tass, Phys. Rev. Lett. **100**, 044105 (2008).
[6] G. C. Sethia, A. Sen, and F. M. Atay, Phys. Rev. Lett. **100**, 144102 (2008).
[7] G. Bordyugov, A. Pikovsky, and M. Rosenblum, Phys. Rev. E **82**, 035205 (2010).
[8] C. R. Laing, Phys. D (Amsterdam, Neth.) **238**, 1569 (2009); Chaos **19**, 013113 (2009).
[9] E. A. Martens, C. R. Laing, and S. H. Strogatz, Phys. Rev. Lett. **104**, 044101 (2010).
[10] M. Wolfrum, O. E. Omelchenko, S. Yanchuk, and Y. L. Maistrenko, Chaos **21**, 013112 (2011).
[11] C. R. Laing, K. Rajendran, and I. G. Kevrekidis, Chaos **22**, 013132 (2012).
[12] Y. Zhu, Y. Li, M. Zhang, and J. Yang, Europhys. Lett. **97**, 10009 (2012).
[13] M. J. Panaggio and D. M. Abrams, Phys. Rev. Lett. **110**, 094102 (2013).
[14] D. Dudkowski, Y. Maistrenko, and T. Kapitaniak, Phys. Rev. E **90**, 032920 (2014).
[15] I. Omelchenko, A. Provata, J. Hizanidis, E. Schöll, and P. Hövel, Phys. Rev. E **91**, 022917 (2015).
[16] P. Jaros, Y. Maistrenko, and T. Kapitaniak, Phys. Rev. E **91**, 022907 (2015).
[17] F. Böhm, A. Zakharova, E. Schöll, and K. Lüdge, Phys. Rev. E **91**, 040901 (2015).
[18] D. M. Abrams and S. H. Strogatz, Phys. Rev. Lett. **93**, 174102 (2004).
[19] N. C. Rattenborg, C. J. Amlaner, and S. L. Lima, Neurosci. Biobehav. Rev. **24**, 817 (2000).
[20] C. G. Mathews, J. A. Lesku, S. L. Lima, and C. J. Amlaner, Ethology **112**, 286 (2006).
[21] D. M. Abrams, R. Mirollo, S. H. Strogatz, and D. A. Wiley, Phys. Rev. Lett. **101**, 084103 (2008).
[22] A. Pikovsky and M. Rosenblum, Phys. Rev. Lett. **101**, 264103 (2008).
[23] R. Ma, J. Wang, and Z. Liu, Europhys. Lett. **91**, 40006 (2010).
[24] M. R. Tinsley, S. Nkomo, and K. Showalter, Nat. Phys. **8**, 662 (2012).
[25] A. M. Hagerstrom, T. E. Murphy, R. Roy, P. Hövel, I. Omelchenko, and E. Schöll, Nat. Phys. **8**, 658 (2012).
[26] E. A. Viktorov, T. Habruseva, S. P. Hegarty, G. Huyet, and B. Kelleher, Phys. Rev. Lett. **112**, 224101 (2014).
[27] M. Wickramasinghe and I. Z. Kiss, Phys. Chem. Chem. Phys. **16**, 18360 (2014).
[28] E. A. Martens, S. Thutupalli, A. Fourrire, and O. Hallatschek, Proc. Natl. Acad. Sci. USA **110**, 10563 (2013).
[29] L. Larger, B. Penkovsky, and Y. Maistrenko, Phys. Rev. Lett. **111**, 054103 (2013).
[30] K. Schönleber, C. Zensen, A. Heinrich, and K. Krischer, New J. Phys. **16**, 063024 (2014).
[31] S. H. Strogatz, C. M. Marcus, R. M. Westervelt, and R. E. Mirollo, Phys. D (Amsterdam, Neth.) **36**, 23 (1989).
[32] H.-A. Tanaka, A. J. Lichtenberg, and S. Oishi, Phys. D (Amsterdam, Neth.) **100**, 279 (1997).
[33] D. Pazó, Phys. Rev. E **72**, 046211 (2005).
[34] J. Gómez-Gardeñes, S. Gómez, A. Arenas, and Y. Moreno, Phys. Rev. Lett. **106**, 128701 (2011).
[35] L. M. Pecora and T. L. Carroll, Phys. Rev. Lett. **80**, 2109 (1998).
[36] I. Leyva, R. Sevilla-Escoboza, J. M. Buldú, I. Sendiña-Nadal, J. Gómez-Gardeñes, A. Arenas, Y. Moreno, S. Gómez, R. Jaimes-Reategui, and S. Boccaletti, Phys. Rev. Lett. **108**, 168702 (2012).
[37] T. K. D. M. Peron and F. A. Rodrigues, Phys. Rev. E **86**, 056108 (2012).
[38] B. C. Coutinho, A. V. Goltsev, S. N. Dorogovtsev, and J. F. F. Mendes, Phys. Rev. E **87**, 032106 (2013).
[39] W. Liu, Y. Wu, J. Xiao, and M. Zhan, Europhys. Lett. **101**, 38002 (2013).
[40] P. Ji, T. K. D. M. Peron, P. J. Menck, F. A. Rodrigues, and J. Kurths, Phys. Rev. Lett. **110**, 218701 (2013).
[41] X. Zhang, X. Hu, J. Kurths, and Z. Liu, Phys. Rev. E **88**, 010802(R) (2013).
[42] I. Leyva, A. Navas, I. Sendiña-Nadal, J. A. Almendral, J. M. Buldú, M. Zanin, D. Papo, and S. Boccaletti, Sci. Rep. **3**, 1281 (2013).
[43] X. Zhang, Y. Zou, S. Boccaletti, and Z. Liu, Sci. Rep. **4**, 5200 (2014).
[44] G. Su, Z. Ruan, S. Guan, and Z. Liu, Europhys. Lett. **103**, 48004 (2013).
[45] X. Hu, S. Boccaletti, W. Huang, X. Zhang, Z. Liu, S. Guan, and C. Lai, Sci. Rep. **4**, 7262 (2014).
[46] Y. Zou, T. Pereira, M. Small, Z. Liu, and J. Kurths, Phys. Rev. Lett. **112**, 114102 (2014).
[47] W. Zhou, L. Chen, H. Bi, X. Hu, Z. Liu, and S. Guan, Phys. Rev. E **92**, 012812 (2015).

[48] X. Zhang, S. Boccaletti, S. Guan, and Z. Liu, Phys. Rev. Lett. **114**, 038701 (2015).
[49] E. A. Martens, M. J. Panaggio, and D. M. Abrams, New J. Phys. **18**, 022002 (2016).
[50] Y. Feng and H. Hong, Chin. Phys. Lett. **32**, 060502 (2015).
[51] S. Watanabe and S. H. Strogatz, Phys. D (Amsterdam, Neth.) **74**, 197 (1994).
[52] P. Mccullagh, Ann. Stat. **24**, 787 (1996).